JOURNAL OF CATALYSIS **167,** 43–56 (1997)
ARTICLE NO. CA971533

The Reaction Mechanism of the Partial Oxidation of Methane to Synthesis Gas: A Transient Kinetic Study over Rhodium and a Comparison with Platinum

E. P. J. Mallens, J. H. B. J. Hoebink, and G. B. Marin

Schuit Institute of Catalysis, Laboratorium voor Chemische Technologie, Eindhoven University of Technology, P.O. Box 513, 5600 MB Eindhoven, The Netherlands

Received December 8, 1995; revised September 23, 1996; accepted November 14, 1996

The partial oxidation of methane to synthesis gas over rhodium sponge has been investigated by admitting pulses of pure methane and pure oxygen as well as mixtures of methane and oxygen to rhodium sponge at temperatures from 873 to 1023 K. Moreover, pulses of oxygen followed by methane and vice versa as well as pulses of mixtures of methane and labelled oxygen were applied to study the role of chemisorbed oxygen and incorporated oxygen in the reaction mechanism. The decomposition of methane on reduced rhodium results in the formation of carbon and hydrogen adatoms. During the interaction of pure dioxygen with rhodium the catalyst is almost completely oxidized to Rh_2O_3. In addition to rhodium oxide, oxygen is also present in the form of chemisorbed oxygen species. During the simultaneous interaction of methane and dioxygen at a stoichiometric feed ratio and a temperature of 973 K only 0.4 wt% Rh_2O_3 is present. The chemisorbed oxygen species are completely desorbed after 2 s. A Mars–Van Krevelen mechanism is postulated: methane reduces the rhodium oxide, which is reoxidized by dioxygen. Synthesis gas is produced as primary product. Hydrogen is formed via the associative desorption of two hydrogen adatoms from reduced rhodium and the reaction between carbon adatoms and oxygen present as rhodium oxide results in the formation of carbon monoxide. The consecutive oxidation of CO and H_2 proceeds via both chemisorbed oxygen and oxygen present as rhodium oxide. Continuous flow experiments were performed to compare rhodium and platinum. When compared to platinum, rhodium shows a higher conversion to methane at a comparable temperature and also a higher selectivity to both CO and H_2, the difference for CO being most pronounced. The observed differences in methane conversion and selectivities for the two catalysts are ascribed to the higher activation energy for methane decomposition on platinum compared to rhodium. An additional explanation for the difference in H_2 selectivity could be the higher activation energy for OH formation on rhodium compared to platinum.

INTRODUCTION

Synthesis gas, a mixture of CO and H_2, is used as feedstock for many important industrial processes, such as methanol production or the Fischer–Tropsch process. Presently, the most important industrial route to synthesis gas is steam reforming of methane. A promising alternative for the production of synthesis gas is the partial oxidation of methane over supported transition metals due to the more favorable H_2 to CO ratio in the product gas as well as the mild exothermicity of the reaction.

Prettre *et al.* (1) were among the first to report formation of synthesis gas by catalytic conversion of CH_4/O_2 mixtures at a stoichiometric feed ratio, i.e., a methane to oxygen feed molar ratio of 2, over 10 wt% refractory supported Ni at temperatures in the range of 973 to 1173 K. Thermodynamic equilibrium was achieved under all conditions studied, corresponding to the catalyst bed exit temperature. The reaction was reported to occur in two stages. In the first stage methane is converted to CO_2 and H_2O until complete conversion of oxygen is achieved, since oxygen is the limiting reactant at a stoichiometric feed ratio. In the second stage synthesis gas is produced via secondary reactions such as the carbon dioxide and steam-reforming reaction.

A similar mechanism has been proposed for the partial oxidation of methane over 25 wt% Ni/Al_2O_3 (2), mixed metal oxides of Ru (3), various supported transition metals (4, 5), and various supported nickel catalysts (6).

Baerns and co-workers (7, 8) investigated the partial oxidation of methane over 1 wt% $Rh/\gamma\text{-}Al_2O_3$ at a temperature of 1000 K. A surface carbon species and CO_2 are postulated to be the primary reaction products formed by the reaction of methane with reduced and oxidized surface sites. Formation of CO proceeds via a fast reaction between surface carbon species and CO_2, i.e., the reversed Boudouard reaction. Furthermore, OH groups on the support are also considered to be involved in the CH_x conversion to CO via a reforming reaction.

Choudhary *et al.* (9–13) report selectivities to synthesis gas higher than the values predicted by thermodynamic equilibrium in the partial oxidation of methane over NiO–CaO (9), 18.7 wt% Ni/Al_2O_3 (10), Ni/Yb_2O_3 (11), CoO/rare earth oxides (12), and CoO/MgO (13) at temperatures lower than 973 K and a residence time of 10^{-2} s. The

0021-9517/97 $25.00

authors attribute this observation to primary formation of synthesis gas. However, Dissanayake *et al.* (14) report that a difference between the measured and the actual reaction temperature also provides an explanation for the observed difference in selectivities.

Formation of CO and H_2 as primary reaction products in the partial oxidation of methane is reported by Hickman and Schmidt (15–17) applying adiabatically operated monoliths containing a platinum or rhodium catalyst at outlet temperatures around 1300 K and residence times between 10^{-4} and 10^{-2} s. Simulations carried out on the basis of a model consisting of 19 elementary reaction steps provided a theoretical basis for this observation (18).

Parallel formation of CO and CO_2 during the partial oxidation of methane is reported by Lapszewicz and Jiang (19) for transition metal(s) supported on metal oxide(s) and Matsumura and Moffat (20) applying a 10 wt% Ru/SiO_2 catalyst.

The interaction of dioxygen with rhodium and the formation of an oxide phase is of interest in the partial oxidation of methane. Formation of Rh_2O_3 is reported by various authors during the treatment of rhodium with dioxygen or air at various pressures and temperatures. Salanov and Savchenko (21–24) investigated the interaction of oxygen with Rh(100) and polycrystalline rhodium. At oxygen pressures below 10^{-5} Pa and temperatures between 400 and 1600 K oxygen can occur in various states, depending on the surface coverage (21, 22), namely chemisorbed on the surface, penetrated into the near-surface layer of the metal and as part of surface oxide islands. At oxygen pressures higher than 0.1 Pa up to 1000 Pa and temperatures between 400 and 600 K formation of a bulk Rh_2O_3 phase is reported (23, 24). Peuckert (25) studied the oxidation of polycrystalline rhodium at 870 K and an oxygen pressure of 10^5 Pa. The surface was analyzed by means of X-ray photoelectron spectroscopy and it was concluded that a Rh_2O_3 phase was formed. Wang and Schmidt (26) investigated the surface composition of rhodium particles on planar amorphous SiO_2 following treatment at atmospheric pressure and various temperatures in air or H_2. A complete oxidation to Rh_2O_3 is reported as a result of a treatment with air at 773 K. The oxidation kinetics of rhodium in air at 10^5 Pa in the temperature range of 873 to 1273 K was studied by Carol and Mann (27) and formation and growth of Rh_2O_3 was reported. Two structures, a hexagonal and an orthorhombic crystal structure, control the nature of the oxidation kinetics. Beck *et al.* (28) studied changes in the local structure of rhodium oxide particles in a Rh/Al_2O_3 catalyst caused by treatment in dioxygen at atmospheric pressure and temperatures in the range of 800 to 1400 K. A complete oxidation of rhodium to Rh_2O_3 was reported at temperatures at or above 800 K and the Rh_2O_3 particles have a structure similar to orthorhombic Rh_2O_3. Kellog (29, 30) reported formation of stoichiometric Rh_2O_3 on rhodium surfaces at temperatures of 500 K and higher at an oxygen pressure of 130 Pa.

The reduction characteristics of Rh_2O_3 are also of interest. According to Peuckert (25) the decomposition of the Rh_2O_3 phase proceeds via a mixed phase of metallic rhodium and Rh_2O_3. Treatment of Rh_2O_3 particles in hydrogen at 423 K results in complete reduction to rhodium metal, as reported by Wang and Schmidt (26). Rh_2O_3 was also reduced by CO at a pressure of 133 Pa at temperatures above 420 K, as reported by Kellog (30). Oh and Carpenter (31) investigated the oxidation state of rhodium following pretreatment with several gases between 500 and 800 K. The oxidation state of supported rhodium changed reversibly in response to a change in the stoichiometry of its gaseous environment. The catalyst surface was observed to consist mainly of Rh_2O_3 in a net-oxidizing environment, while in the case of a net-reducing stream mainly metallic rhodium is present.

The objective of the present study is to investigate the reaction mechanism of the partial oxidation of methane to synthesis gas over rhodium by means of a transient kinetic study. A Temporal Analysis of Products (TAP) set-up was applied, which allows one to introduce pulses of gases into a reactor. The amount of molecules can be varied between 10^{14} and 10^{18} per pulse and the width of the inlet pulse typically amounts to 0.2 ms. Thermodynamic calculations on the system oxygen–rhodium were performed to assess the possible formation of an oxide phase under the experimental conditions, from a thermodynamic point of view. Both the separate and the simultaneous interaction of methane and dioxygen with the catalyst as well as the reactivity of different oxygen species in the partial oxidation of methane were studied. The emphasis was put on obtaining information concerning these phenomena on a catalyst which was at steady state with an environment as typical as possible for the partial oxidation, i.e., a temperature of 1100 K and a gas phase consisting of methane and oxygen in a feed molar ratio of 2. The reaction paths are analyzed in terms of primary and secondary product formation and a detailed reaction mechanism is proposed. Knudsen diffusion, combined with adsorption and desorption processes are simulated by integrating the continuity equations for the reaction products in order to avoid interference of the latter with the reaction network analysis. The results are compared to previous work involving platinum as the catalyst (32).

EXPERIMENTAL

Equipment and Procedures

The TAP set-up has been described in detail elsewhere (33). The microreactor of the TAP set-up is a batchwise operated fixed bed reactor with a typical residence time of 100 ms. Mass spectrometry is used to follow the outlet

reponses toward pulses of reactants admitted at the inlet with a submillisecond time resolution. It allows one to study catalytic sequences in detail, even at a high conversion. A limited amount of molecules is admitted to the catalyst surface leading to information about the reactants and products at a well defined state of the surface.

The shape of a response is determined by the various processes occurring in the microreactor, namely Knudsen diffusion, adsorption, desorption, and reaction. Each response has a unique rise time, peak maximum, and decay curve.

A plot of the responses as a function of time contains in principle information on the reaction network. A secondary product has a response with a larger rise time than a primary product and its peak maximum is observed later. Adsorption and desorption processes result in a shift of the peak maximum toward a larger time value. The position of the peak maximum is also determined by the molecular weight of the component via the Knudsen diffusion coefficient.

The continuous flow mode of operation of the microreactor was applied for the pretreatment of the catalyst and determination of the absolute calibration factors. The latter allows one to convert the mass spectrometer signal into moles per second. The total flow in a continuous flow experiment amounts to $2\,10^{-7}$ mol s^{-1}, resulting in an average pressure in the microreactor in the order of 10^4 Pa.

Transient experiments were performed in three different ways. The first type is referred to as a **pulse experiment**, during which the response to a single pulse is monitored at a fixed atomic mass unit (AMU) value.

The second type is referred to as an **alternating pulse experiment**, also called pump-probe experiment (33). Two single pulses are introduced and the response is measured at a fixed AMU value. By varying the time interval between the two single pulses information on the lifetime and reactivity of adsorbed species is obtained. These species are created during the first single pulse and probed with a suitable reactant during the second single pulse.

In both a pulse and an alternating pulse experiment pulses are repeated regularly and the responses are averaged to improve the signal-to-noise ratio. The repetition time is chosen sufficiently large to avoid accumulation of adsorbed species at the surface. This sequence is repeated for each AMU value to be measured.

The third type concerns a **multipulse experiment.** A series of single pulses is introduced and the responses of all pulses are monitored separately, i.e., without signal averaging, at a fixed AMU value. The time interval between two single pulses is variable and must be larger than the average residence time in the reactor to avoid accumulation of components in the void space of the catalyst bed. A multipulse experiment can be used to study the interacion of a component with the surface at different degrees of surface coverage.

The number of molecules admitted per single pulse was in the range of 10^{15}–10^{16}, resulting in an average total pressure of 100 Pa above the catalyst surface during 100 ms. Gas phase reactions can be neglected under these conditions. In a single pulse the ratio of admitted methane as well as oxygen molecules to the theoretical number of surface rhodium atoms was always below 0.05. The background pressure in the reactor section of the set-up amounts to 10^{-5} Pa.

The inconel microreactor, with a length of 42 mm and an inner diameter of 6 mm, was charged with 0.07 to 0.2 g of catalyst and packed with inert material at each end. Two thermocouples were inserted into the catalyst bed for temperature measurements. The axial temperature difference over the bed was always limited to 5 K.

The experiments were carried out in the temperature range of 873 to 1023 K. The detected reaction products were H_2, CO, H_2O, and CO_2. No formation of C_2-products was observed. For each experiment the conversion and selectivities as well as carbon, hydrogen, and oxygen balances were calculated, according to the following equations.

$$X_{CH_4} = \frac{n_{in,CH_4} - n_{out,CH_4}}{n_{in,CH_4}} \quad [1]$$

$$S_{H_2} = \frac{n_{out,H_2}}{n_{out,H_2} + n_{out,H_2O}} \quad [2]$$

$$S_{CO} = \frac{n_{out,CO}}{n_{out,CO} + n_{out,CO_2}} \quad [3]$$

$$\epsilon_C = \frac{n_{out,CH_4} + n_{out,CO} + n_{out,CO_2} - n_{in,CH_4}}{n_{in,CH_4}} \quad [4]$$

$$\epsilon_O = \frac{2n_{out,O_2} + n_{out,CO} + 2n_{out,CO_2} + n_{out,H_2O} - 2n_{in,O_2}}{2n_{in,O_2}} \quad [5]$$

$$\epsilon_H = \frac{4n_{out,CH_4} + 2n_{out,H_2} + 2n_{out,H_2O} - 4n_{in,CH_4}}{4n_{in,CH_4}}, \quad [6]$$

where X is the conversion (mol mol^{-1}), S is the selectivity (mol mol^{-1}), n is the total amount of moles (mol), and ϵ is the mass balance (mol mol^{-1}).

The carbon, hydrogen, and oxygen balances always showed an accuracy better than 8%. Errors up to 15% are considered to be acceptable in view of the accuracy of the absolute calibration factor. The conversion of methane was always nearly complete, unless specified otherwise.

Apparent activation energies for the interaction of oxygen and methane with the catalyst were derived from the linear dependence of ln X on the inverse temperature, applying an identical amount of molecules per pulse at various temperatures. Only experiments in which the conversion is lower than 50% were selected for determination of the activation energies.

Materials

The gases used were methane (99.9995%), oxygen (99.995%), carbon monoxide (99.9997%), carbon dioxide (99.995%), hydrogen (99.999%), and argon (99.99995%) from Air Products. Labelled oxygen, $^{18}O_2$ (99.5%) from Union Carbide was used as well.

The catalysts applied were rhodium sponge (99.9%) and platinum sponge (99.9%), both from Johnson Matthey, with a grain diameter of 0.25 to 0.35 mm. The BET surface area of the fresh rhodium catalyst amounted to 0.25 $m^2\ g^{-1}$ and for the fresh platinum catalyst to 0.05 $m^2\ g^{-1}$. These surface areas correspond to diameters of the primary nonporous particles forming the porous grain of 5 μm for platinum and 2 μm for rhodium. Nonporous α-Al_2O_3 with a grain diameter of 0.25 to 0.30 mm was used as inert packing material. The catalyst has two important advantages for the present study. No support is used to avoid interactions between the metal and a support material as well as interactions between reactants or reaction products and a support material. Second, the time scale for Knudsen diffusion in the interstitial voids is 100 times the time scale of Knudsen diffusion in the intragranular voids. This means that the shape of the response is not influenced by intragranular diffusion (34).

Blank pulse experiments of methane as well as methane with oxygen over α-Al_2O_3 showed a conversion of 2%, which is negligible compared to conversions obtained in the presence of a catalyst. In all experiments argon was added to the admitted gases as a reference component for calculation of the conversion of the reactants and the amount of admitted molecules.

The amount of surface metal atoms and of metal oxide was determined *in situ*. The former followed from a multipulse experiment of oxygen at a temperature of 373 K over a surface covered with carbon monoxide. The responses of carbon dioxide were monitored and their cumulative surface area provided the amount of carbon dioxide molecules formed which is considered identical to the number of surface metal atoms. The specific surface area based on a theoretical amount of 1.32×10^{19} rhodium atoms per square meter and of 1.30×10^{19} platinum atoms per square meter, was found to be identical to that determined *ex situ* by the BET method. The amount of metal oxide was determined by both a continuous flow and a multipulse experiment of hydrogen. The response of water was measured from which the amount of incorporated oxygen was deduced. In the case of a multipulse experiment typical 200 pulses of hydrogen are introduced, during which the number of molecules per pulse is in the range of 10^{16}–10^{17}. For a continuous flow experiment a flow of 10^{-7}–10^{-6} mol s^{-1} is applied. In both cases the experiment is continued until the water production is negligible. Integration of the water response yields the total amount of atomic oxygen present as metal oxide. Repetition of a multipulse reduction at various time intervals after the experiment did not show water formation, from which it is concluded that complete reduction has occurred.

The catalyst was pretreated *in situ* for 2 h at a temperature of 1123 K with a continuous flow of a mixture of 80 vol% oxygen in argon, followed by a flow of 80 vol% hydrogen in argon. After the pretreatment the specific surface area had decreased to 0.23 $m^2\ g^{-1}$ for rhodium and to 0.035 $m^2\ g^{-1}$ for platinum. These values remained constant during the various subsequent experiments.

Prior to each transient experiment, as defined above, the catalyst was treated with a continuous flow of methane and oxygen, unless mentioned otherwise, in the same feed molar ratio as the following experiment, after which it was kept under a pressure of 10^{-5} Pa for 5 min.

MODEL EQUATIONS FOR THE SIMULATION OF ADSORPTION, DESORPTION, AND KNUDSEN DIFFUSION PROCESSES

The outlet flow rates of the four reaction products were calculated by integrating the corresponding continuity equations for a single pulse of an equimolar mixture of CO, CO_2, H_2, and H_2O and corresponding Knudsen diffusion, adsorption, and desorption coefficients to investigate the influence of these processes on the shape of the responses. Reaction is not included in the simulations. Comparison of these simulation results with the results obtained by simultaneous pulsing of methane and oxygen allows one to ascertain that the above phenomena do not disguise the reaction network analysis of the partial oxidation of methane to synthesis gas.

In general when studying a catalytic reaction with the TAP set-up, the microreactor will be packed with three subsequent beds. The response after injection of a gas pulse is a function of all processes appearing in the reactor, gas transport, adsorption, desorption, and reaction, and can be simulated by integrating the continuity equations for all components considered. When the catalyst bed is placed in the isothermal part of the reactor, the energy balances can be omitted. In the present analysis, the only processes taken into consideration are diffusion, adsorption, and desorption.

It is assumed that the only transport mechanism of molecules through the reactor is Knudsen diffusion. This assumption is valid since the amount of molecules per pulse was always below 10^{16} and under these conditions Knudsen diffusion is the dominant transport mechanism (34). The effective Knudsen diffusion coefficient of component A, is calculated as

$$D^{\kappa}_{e,A} = \frac{\varepsilon_b}{\tau_b}\frac{d_i}{3}\sqrt{\frac{8RT}{\pi M_A}}, \qquad [7]$$

where $D^{\kappa}_{e,a}$ is the effective Knudsen diffusion coefficient ($m_g^3\ m_r^{-1}\ s^{-1}$), ε_b is the bed porosity (0.6 $m_g^3\ m_r^{-3}$), τ_b is the bed tortuosity (5.6 $m_g^2\ m_r^{-2}$), d_i is the diameter of the

interstitial voids (m), R is the general gas constant (J mol^{-1} K^{-1}), T is the temperature (K), and M_A is the molecular mass (kg mol^{-1}).

The diameter of the intersitial voids, d_i, follows from the definition for the hydraulic diameter (35). The continuity equations are shown for a general case of component A, showing first order adsorption and desorption:

$$A + * \underset{k_{des}}{\overset{k_{ads}}{\rightleftarrows}} A*, \qquad [8]$$

where $*$ signifies an adsorption site. The gas phase concentration profile of component A as function of the reactor coordinate can be calculated by integrating the continuity equations for component A in each of the packed beds, i.e., two inert beds and one catalyst bed. Only the balances for the catalyst bed are presented here. In the case of the inert beds the reaction terms in the continuity equations can be put equal to zero.

The continuity equations for the gas phase component A and the corresponding adsorbed species over the catalyst bed as well as the initial and boundary conditions are

$$\varepsilon_b \frac{\partial C_A}{\partial t} = D^{\kappa}_{e,A} \frac{\partial^2 C_A}{\partial x^2} + (1-\varepsilon_b) a_v L_t (-k_{ads} C_A (1-\theta_A) + k_{des}\theta_A) \qquad [9]$$

$$\frac{\partial \theta_A}{\partial t} = k_{ads} C_A (1-\theta_A) - k_{des}\theta_A. \qquad [10]$$

The initial conditions follow from the initial gas phase concentration and the initial surface coverage of component A:

$$t = 0 \wedge 0 \le x \le l_b \,:\, C_A(x) = \delta_x \frac{N_{p,A}}{\varepsilon_b A_s} \qquad [11]$$

$$t = 0 \wedge 0 \le x \le l_b \,:\, \theta_A(x) = 0. \qquad [12]$$

The two boundary conditions are shown below. After the introduction of the gas pulse, the pulse valve is closed meaning a zero flux at the reactor entrance:

$$t \ge 0 \wedge x = 0 : \frac{\partial C_A}{\partial x} = 0. \qquad [13]$$

The concentration for component A at the end of the catalyst bed can be put equal to zero, because the reactor outlet is maintained at a pressure of 10^{-5} Pa:

$$t \ge 0 \wedge x = l_b \,:\, C_A = 0, \qquad [14]$$

where a_v, is the external catalyst surface area per unit catalyst volume (8.9 10^5 m_c^2 m_c^{-3}), L_t is the maximal molar concentration per square meter of catalyst surface (2.2 10^5 mol m_c^{-2}), θ is the fractional coverage on the surface (-), k_{ads} is the adsorption rate coefficient, and k_{des} is the desorption rate coefficient.

The partial differential equations with the accompanying initial and boundary conditions were integrated numerically with the routine D03PGF from the NAG Fortran Library, as described by Huinink (34). The Knudsen diffusion coefficients were calculated using the relationship given by Eq. [7], for a particle diameter of 300 μm. The values for the adsorption and desorption rate coefficients are obtained from Hickman and Schmidt (15), since these values are taken from studies on unsupported single crystals as well as polycrystalline catalyst studies. The adsorption and desorption of CO_2 are neglected in their model.

The results of the simulations are shown in Fig. 1, which shows the normalized responses of hydrogen, water, carbon monoxide, and carbon dioxide when Knudsen diffusion, adsorption, and desorption are considered. In this case the response of water is observed prior to that of hydrogen and the response of carbon dioxide is observed prior to that of carbon monoxide.

The shape of the responses can be explained qualitatively by comparison of the characteristic times of Knudsen diffusion, adsorption, and desorption for hydrogen, water, and carbon monoxide. These values are calculated by

$$\tau_{diff} = \frac{l_b^2\, \varepsilon_b}{2 D^{\kappa}_{e,A}} \qquad [15]$$

$$\tau_{ads} = \frac{\varepsilon_b}{(1-\varepsilon_b) a_v L_t k_{ads} \theta_*} \qquad [16]$$

$$\tau_{des} = \frac{1}{k_{des}}, \qquad [17]$$

where τ_{diff}, τ_{ads}, and τ_{des} are the characteristic times for Knudsen diffusion, adsorption, and desorption, respectively.

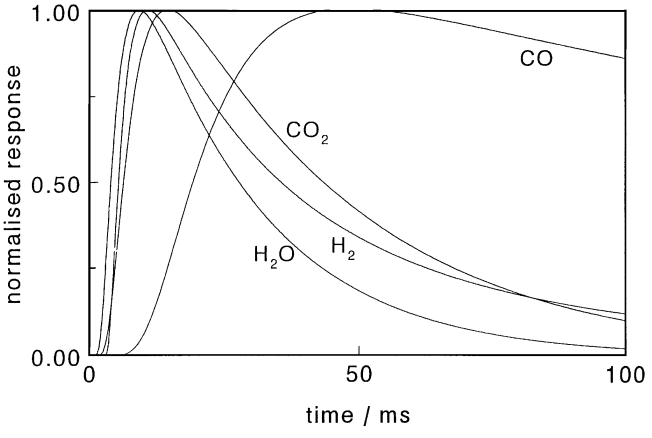

FIG. 1. Normalized responses of H_2 (×1.72), H_2O, CO (×10.14), and CO_2(×1.59) as a function of time. Simulation of Knudsen diffusion, adsorption, and desorption over rhodium sponge by integrating continuity Eqs. [9] and [10] with initial and boundary conditions [11–14].

TABLE 1

Characteristic Times for Knudsen Diffusion, Adsorption, and Desorption of Various Gases on Rhodium Sponge at a Temperature of 973 K

Process	Characteristic time (s)		
	H_2	H_2O	CO
Knudsen diffusion	1.4×10^{-2}	2.3×10^{-2}	2.9×10^{-2}
Adsorption	5.6×10^{-9}	1.7×10^{-8}	6.5×10^{-9}
Desorption	2.2×10^{-9}	2.7×10^{-11}	3.1×10^{-7}

The results are shown in Table 1 for a total bed length of 25×10^{-3} mm and a temperature of 973 K. In the case of hydrogen an adsorption equilibrium can be expected which explains the broadening of the hydrogen response due to adsorption and desorption phenomena. For carbon monoxide the relatively slow desorption from the surface causes the large broadening of the response. In the case of water the response resembles that determined by diffusion alone, becuase the equilibrium is on the side of gaseous water.

THERMODYNAMIC EVALUATION OF THE SYSTEM OXYGEN–RHODIUM

In order to obtain insight into the thermodynamic stability of the possible species in the system oxygen–rhodium, thermodynamic calculations were performed at 1000 K.

The species to be considered in the thermodynamic equilibrium calculations are $O_{2(g)}$, $Rh_{(c)}$, $Rh_{(g)}$, $Rh_2O_{(c)}$, $RhO_{(c)}$, $Rh_2O_{3(c)}$, and $RhO_{2(g)}$, according to Schäfer *et al.* (36), Alcock and Hooper (37) and Barin (38). A convenient representation of systems involving three gaseous species is possible in a so-called volatility diagram. Volatility diagrams show the activities of two gaseous species in equilibrium with the condensed phases at a given temperature. The construction and use of this type of diagram is discussed by Heuer (39) and Lou *et al.* (40) Thermodynamic data from Barin (38), Barin and Knacke (41), and Alcock and Hooper (37) are used in the calculations.

The following basic assumptions were used in the thermodynamic calculations: (i) the condensed phases are pure and stoichiometric and (ii) the partial molar volume of gas phase components is much larger than that for solid phase components. As a result of these two assumptions the chemical potential of a condensed component is equal to its standard chemical potential, which is only a function of the temperature. Furthermore, a constant pressure is assumed in the calculations.

The volatility diagram for the system oxygen–rhodium at a temperature of 1000 K is shown in Fig. 2. The volatility diagram consists of four fields, assigned to $Rh_{(c)}$, $Rh_2O_{(c)}$, $Rh_2O_{3(c)}$ and a gas phase, consisting of $RhO_{2(g)}$, $Rh_{(g)}$, and $O_{2(g)}$. The thermodynamic equilibrium composition of the gas phase is ruled by the equilibrium constant of the reaction

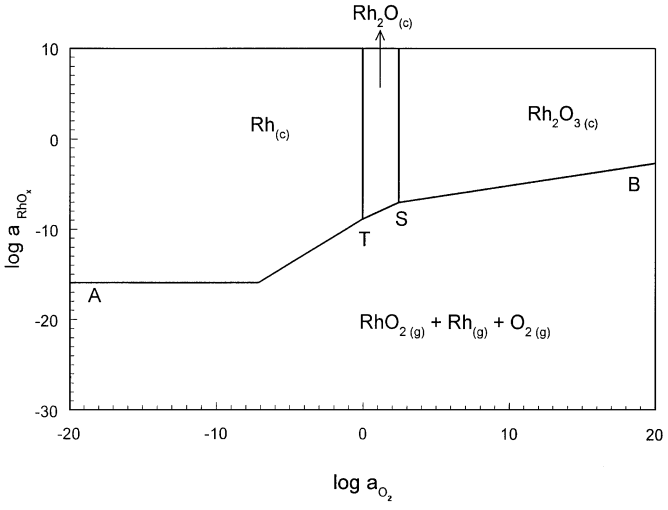

FIG. 2. Volatility diagram of oxygen/rhodium at a temperature of 1000 K and a constant pressure.

$$RhO_{2(g)} \rightleftarrows Rh_{(g)} + O_{2(g)}. \quad [18]$$

At given activity of $O_{2(g)}$ and $Rh_{(g)}$, the activity of $RhO_{2(g)}$ is fixed by the equilibrium of Eq. [18]. The line A to B corresponds to an equilibrium between the gas phase and one or more condensed phases.

The triple points T and S (see Fig. 2) represent the points where three phases are in equlibrium. For example, at triple point T the condensed phases $Rh_{(c)}$ and $Rh_2O_{(c)}$ and the gas phase are in equilibrium, leaving the temperature as the only degree of freedom.

The minimum activity of oxygen necessary for the formation of Rh_2O_3 corresponds to the triple point S and amounts to 250 Pa. During the experimental work with the TAP setup the average pressure of oxygen has a similar order of magnitude and therefore formation of $Rh_2O_{3(c)}$ can be expected from a thermodynamic point of view during the interaction of oxygen with rhodium sponge at temperatures of approximately 1000 K. The field corresponding to Rh_2O_3 as condensed phase becomes smaller with increasing temperature.

EXPERIMENTAL RESULTS

Interaction of Oxygen with Reduced Rhodium

The interaction of oxygen with the catalytic surface was investigated with a continuous flow experiment of oxygen as well as multipulse experiments of oxygen. The catalyst was exposed to a continuous flow of oxygen at a temperature of 1073 K. In this case the catalyst was completely reduced prior to the experiment. Initially oxygen was not detected quantitatively, but the oxygen response increased and finally reached a constant value after a period of 2500 s. The argon response remained constant during this experiment.

The gradual increase in the oxygen response is attributed to the incorporation of oxygen into the catalyst and the ratio of incorporated atomic oxygen to the number of rhodium atoms can be calculated to be 1.7 from the oxygen balance.

A sample of the treated catalyst as well as the fresh rhodium sponge was analyzed ex-situ by means of X-ray diffractometry (XRD) measurements as well as X-ray photoelectron spectroscopy (XPS) measurements. The fresh sample was reduced *in situ* at 973 K by hydrogen for 1 h. After this reduction the sample was cooled to room temperature maintaining a pressure of 10^{-5} Pa. Finally, the sample was transferred to the set-up for analysis. The former analysis showed that the treated sample consisted of stoichiometric Rh_2O_3 as well as metallic rhodium, while the fresh sample consisted solely of metallic rhodium. From the XPS measurements it was concluded that in the case of the treated sample stoichiometric Rh_2O_3 is present and that the ratio of oxidic atomic oxygen to rhodium atoms amounted to 1.7, which is identical to the value obtained from the continuous flow experiments. For the fresh sample solely metallic rhodium was detected. During the continuous flow of oxygen the average pressure of oxygen in the catalyst bed amounts to 10^4 Pa. Thermodynamic calculations (Fig. 2) show that at oxygen pressures of 250 Pa or higher a Rh_2O_3 phase is thermodynamically stable at the investigated temperature. Therefore, the incorporation of oxygen into the catalyst is attributed to the almost complete oxidation of rhodium to Rh_2O_3. A possible explanation for the absence of any surface oxygen in the case of the fresh sample is the structure of the catalyst, consisting of nonporous particles forming the porous grain of 2 μm, instead of a supported rhodium catalyst. This may also explain the partial decomposition of the treated sample, since XRD analysis revealed the presence of both Rh_2O_3 and metallic rhodium. This decomposition does not influence the XPS measurements under the assumptium that due to the diffusion of oxygen to the surface the latter remains oxidised.

The treated catalyst sample was kept for a time interval varying between zero and 1800 s at a pressure of 10^{-5} Pa and a temperature of 898 K, after which multipulse experiments of oxygen were carried out. In a typical experiment 15 pulses were introduced with a 2-s time interval between the pulses. A typical result is shown in Fig. 3. The surface area of the individual oxygen responses increases and finally remains constant. The initial increase is attributed to oxygen incorporation into the catalyst. The amount of incorporated oxygen increases linearly with increasing time at 10^{-5} Pa up to 0.7 theoretical monolayers of atomic oxygen at 1800 s. No constant value is reached as in the case of platinum after maintaining 10^{-5} Pa during at least 300 s (32). A second series of multipulse experiments was carried out at 900 s after interrupting the continuous flow of oxygen but now at temperatures between 875 and 948 K. The amount of incorporated oxygen increases exponentially, expecially above 923 K, up to 5.1 theoretical monolayers of atomic oxygen at 948 K.

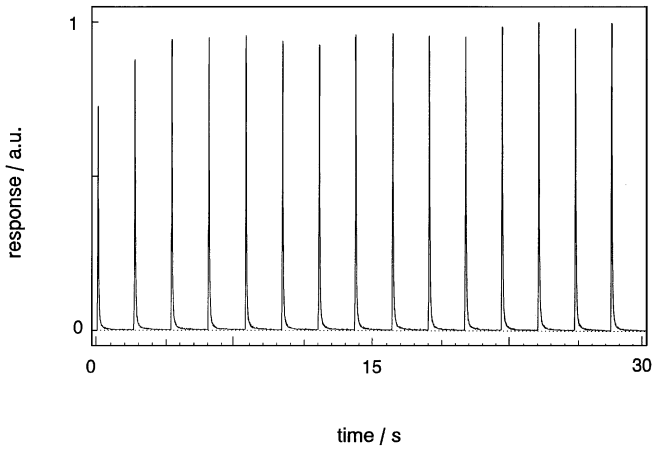

FIG. 3. Response of oxygen as a function of time. Multipulse experiment of oxygen at 873 K over almost completely oxidized rhodium sponge.

The peak maximum of each individual response of oxygen shifts to a larger time value than the peak maximum of the argon response (see Fig. 4), which points to reversible adsorption of oxygen at the catalyst surface. After a time interval of 2 s desorption of dioxygen is no longer observed.

Interaction of Methane with Reduced Rhodium

The interaction of methane with the catalyst was investigated by introducing a single pulse of methane. In this case the catalyst was completely reduced prior to the experiment. Methane and hydrogen responses were monitored at the reactor outlet. No formation of carbon monoxide, carbon dioxide, ethane, and ethene was observed. The residence time of methane amounted to 0.2 s and that of hydrogen to 0.4 s. The carbon balance was significantly negative, while the hydrogen balance was closed within 7% or less,

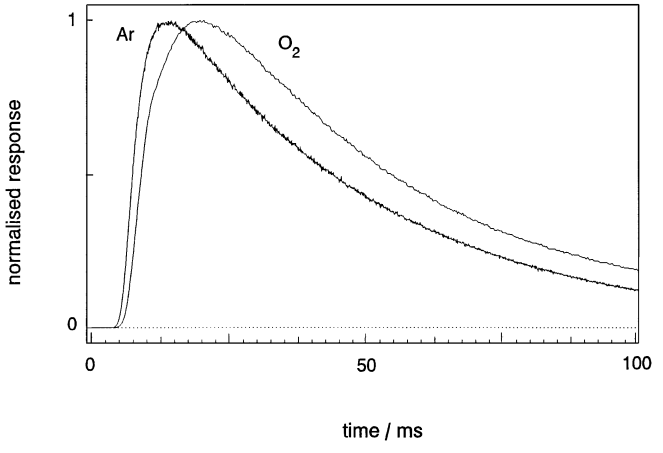

FIG. 4. Normalized responses of argon (×5) and oxygen as a function of time. Pulse experiment of argon and oxygen at 1023 K over almost completely oxidized rhodium sponge.

indicating the formation of carbon adatoms. The conversion of methane increased from 44% at 598 K to 81% at 748 K. The apparent activation energy for methane decomposition amounted to 15 kJ mol^{-1}.

Alternating Pulse Experiments over Rhodium

The role of adsorbed oxygen species was investigated with alternating pulse experiments of oxygen and methane and vice versa. An admitted methane to oxygen molar ratio of 0.5 was used to ensure complete reoxidation of the catalyst. No oxygen was detected quantitatively and the carbon as well as hydrogen balances were always closed. The oxygen balance is not closed at all time intervals applied and some oxygen is incorporated into the catalyst. However, this does not influence the experimental results since this amount is very small compared to the amount of Rh_2O_3 already present. Prior to the experiments the catalyst was treated with a continuous flow of methane and oxygen with a molar feed ratio of 0.5 until a steady state was reached. Product formation was only observed during the methane pulse.

First, an experiment starting with oxygen was carried out. Seven different time intervals between the oxygen and methane pulse were applied, varying from zero, i.e., simultaneous pulsing, up to 9 s. Figure 5 shows the selectivities to H_2 and CO as a function of the time interval between the oxygen and the methane pulse. The selectivity to CO increases from 7% when pulsing simultaneously to 33% at a time interval of 2 s, while the corresponding H_2 selectivity increases from 18 to 58%. The selectivities to CO and H_2 do not vary significantly when the time interval between the methane and oxygen pulse is further increased from 2 s up to 9 s.

Next, an experiment starting with methane was performed, the time interval being varied between zero and

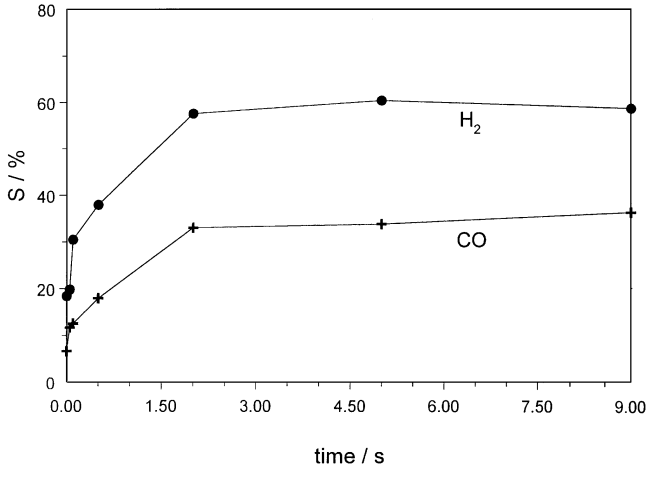

FIG. 5. Selectivities of CO and H_2 as a function of the time interval between the oxygen and methane pulse. Alternating pulse experiment starting with oxygen at 973 K over rhodium sponge (2.1 wt% Rh_2O_3) and a methane to oxygen feed molar ratio of 0.5.

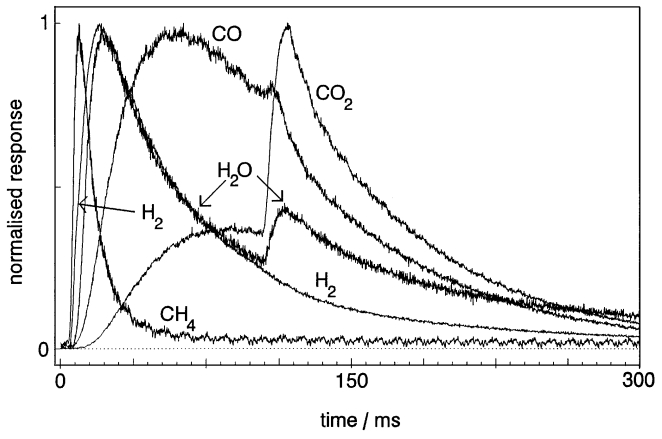

FIG. 6. Normalized responses of CH_4 (×38), CO (×2.4), CO_2 (×1.7), and H_2 and H_2O (×4.3) as a function of time. Alternating pulse experiment starting with methane followed by oxygen at a time interval of 0.1 s. Rhodium sponge (2.1 wt% Rh_2O_3), a methane to oxygen feed molar feed ratio of 0.5 and a temperature of 973 K.

1.0 s. The selectivity to CO increases from 7% when simultaneous pulsing to 46% at a time interval of 0.5 s, while the corresponding selectivity to H_2 increases from 18 to 70%. Increasing the time interval further to 1 s has no influence on the selectivities to CO and H_2. From a time interval of 0.5 s onward the oxygen was introduced into the reactor when gaseous methane was no longer present in the catalyst bed. No formation of carbon-containing reaction products was observed during the interaction of oxygen with the catalyst. The normalized responses of CO, H_2, CO_2, and H_2O applying a time interval of 0.1 s between the methane and oxygen pulse are shown in Fig. 6. The starting point and peak maximum of CO are observed prior to those of CO_2. A similar conclusion can be drawn from the responses of H_2 and H_2O. Furthermore, as soon as oxygen is introduced into the reactor and thus chemisorbed oxygen species are formed, the formation of CO_2 abruptly increases, while that of CO decreases. Similar behavior of the H_2 and H_2O responses is observed, though the effects are less pronounced due to the fact that most gaseous hydrogen has already left the reactor at the moment dioxygen is introduced. At smaller time intervals between the methane and oxygen pulse the decrease in the hydrogen response is much more pronounced.

Simultaneous Interaction of Methane and Oxygen with Rhodium during Pulse Experiments

The simultaneous interaction of methane and oxygen with the catalyst was investigated applying both unlabeled and labeled dioxygen. No oxygen was detected quantitatively and the carbon, hydrogen, and oxygen balances were always closed. The role of oxygen present at Rh_2O_3 versus adsorbed oxygen in the partial oxidation of methane was investigated by a multipulse experiment of CH_4 and $^{18}O_2$ at a stoichiometric feed ratio. Prior to the experiment the

catalyst was treated with a continuous flow of CH_4 and $^{16}O_2$ at a stoichiometric feed ratio, which means that $Rh_2{}^{16}O_3$ is present. Eight pulses of CH_4 and $^{18}O_2$ were introduced into the reactor with a 5-s time interval between the pulses. Formation of H_2 ($S = 95\%$), $H_2{}^{16}O$ ($S = 2.6\%$), $H_2{}^{18}O$ ($S = 2.4\%$), $C^{16}O_2$ ($S = 2.9\%$), and $C^{16}O^{18}O$ ($S = 1.1\%$) was already observed during the first pulse and the selectivities remained the same during the subsequent seven pulses of the multipulse experiment. The selectivities of $C^{16}O$ and $C^{18}O$ as a function of the pulse number are shown in Fig. 7, which is a compilation of the results of two multipulse experiments. Between the two experiments the state of the catalyst was restored by treatment with a continuous flow of CH_4 and $^{16}O_2$ at a stoichiometric feed ratio until no further formation of labeled products was observed. During the first pulse no formation of $C^{18}O$ was observed, (see Fig. 7), and the selectivity increases up to 25% at the eighth pulse. The selectivity to $C^{16}O$ decreases from 96% to 71%, which means that the cumulative selectivity to CO remains constant at a level of 96% during the multipulse experiment. During the first pulse 95% of the ^{18}O was incorporated into the catalyst, which decreases to 70% at the eighth pulse.

Simultaneous pulse experiments of CH_4 and $^{16}O_2$ were carried out 923, 973, and 1023 K at feed molar ratios of 2, 1, and 0.5. Prior to the experiments the catalyst was treated with a continuous flow of CH_4 and O_2 in the same molar as the experiment to follow. The selectivities to CO and H_2 at 973 K increase from 7 and 18% at a ratio of 0.5, to 34 and 64% at a ratio of 1, and finally to 90 and 94% at a ratio of 2. The selectivities to CO and H_2 are hardly influenced by the reaction temperature in the range of 923 to 1023 K.

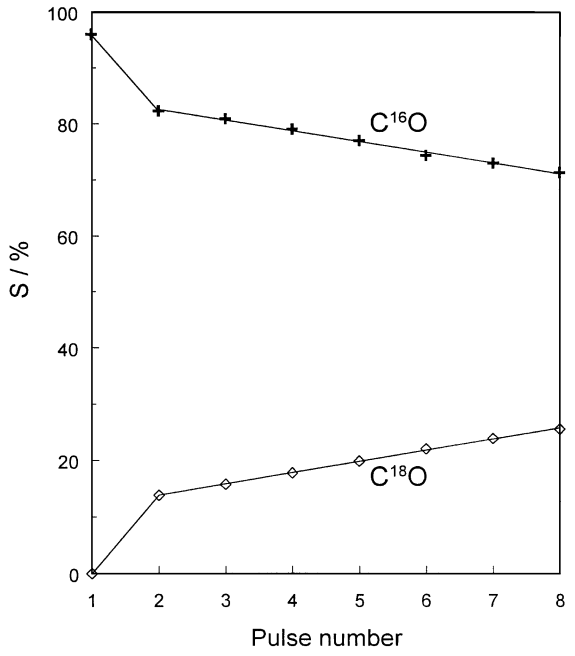

FIG. 7. Selectivities to $C^{16}O$ and $C^{18}O$ as a function of the pulse number. Multipulse experiment of eight pulses of $CH_4/^{18}O_2$ at a feed molar ratio of 2 at 973 K over rhodium sponge (0.4 wt% $Rh_2{}^{16}O_3$).

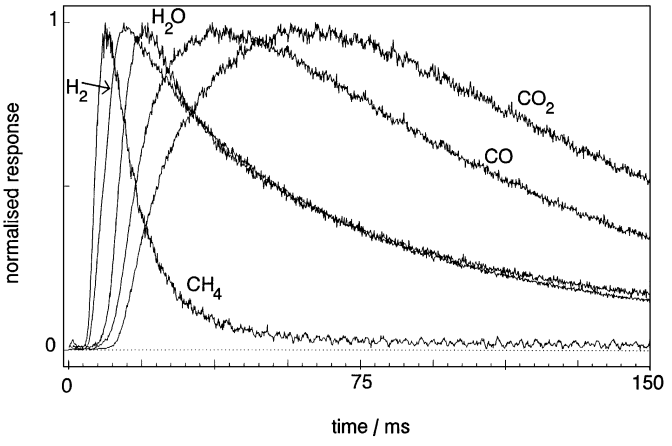

FIG. 8. Normalized responses of CH_4 (×25), CO (×2.9), CO_2 (×12), and H_2 and H_2O (×10) as a function of time. Simultaneous pulse experiments of CH_4/O_2 at a feed molar ratio of 2 over rhodium sponge (0.4 wt% Rh_2O_3) at 973 K.

The normalized responses of CO, CO_2, H_2, and H_2O from a simultaneous pulse experiment of CH_4 and $^{16}O_2$ at a stoichiometric feed ratio at 973 K are shown in Fig. 8. The starting point and maximum of the H_2 response are observed before those of the H_2O response. Furthermore, the starting point and maximum of the CO response are observed before those of the CO_2 response.

Simultaneous Interaction of Methane and Oxygen with Rhodium during Continuous Flow Experiments

Experiments with a continuous flow of methane and oxygen with feed molar ratios of 2, 1, and 0.5 were carried out to investigate the influence of reaction temperature and feed ratio on the conversion and product selectivities. In none of the experiments was dioxygen detected quantitatively nor were C_2-products observed. The carbon, hydrogen, and oxygen balances were closed. The conversion of methane and selectivities of CO and H_2 are shown in Figs. 9 and 10 for a CH_4 to O_2 feed molar ratio of 2. Figure 9 shows that the methane conversion increases from 30% at 773 K to become nearly complete at 973 K. The corresponding selectivities of CO and H_2 increase from 76 and 29% to 100% (see Fig. 10). At a feed molar feed ratio of 1, the conversion of methane increases from 44% at 773 K to 100% at 823 K. The selectivity of H_2 increases from 2% at 773 K to 77% at 823 K and then slightly decreases to 72% at 1023 K, while the selectivity to CO increases from approximately zero up to 49% in the same temperature range. In the case of a CH_4 to O_2 feed molar ratio of 0.5 the conversion of methane is nearly complete and solely CO_2 and H_2O are produced in the temperature range of 773 to 1023 K.

The amount of Rh_2O_3 present during the simultaneous interaction of methane and oxygen was investigated as a

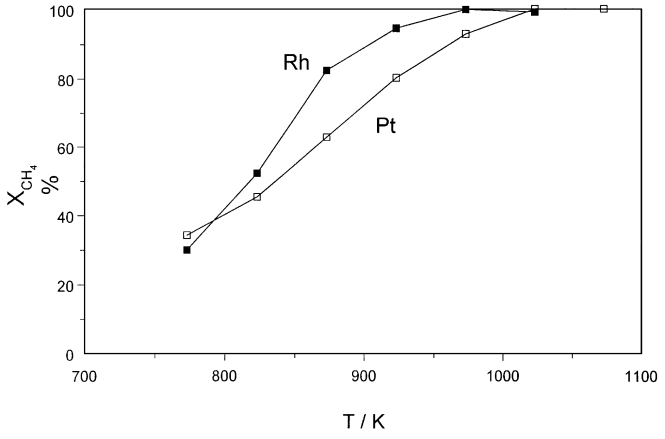

FIG. 9. Conversion of methane as a function of temperature for rhodium (0.4 wt% Rh_2O_3) and platinum sponge (0.9 wt% PtO_2). Continuous flow experiment of CH_4/O_2 at a feed molar ratio of 2. The oxygen conversion was complete in all experiments.

function of the methane to oxygen feed molar ratio at 973 K. As soon as the steady state was reached, the flow of reactants was switched off and the amount of Rh_2O_3 was determined by means of H_2 multipulse reduction. The percentages of rhodium oxidized, assuming an oxide stoichiometry of Rh_2O_3, are shown in Table 2, for the three different CH_4 to O_2 feed molar ratios. The amount of Rh_2O_3 present at reaction conditions increases from 0.4 wt% at a stoichiometric feed ratio to 2.1 wt% at a methane to oxygen feed molar ratio of 0.5 at a temperature of 973 K. The first amounts to 10 theoretical monolayers of atomic oxygen.

Simultaneous Interaction of Methane and Oxygen with Platinum during Continuous Flow Experiments

As for rhodium, experiments with a continuous flow of methane and oxygen with feed molar ratios of 2, 1, and

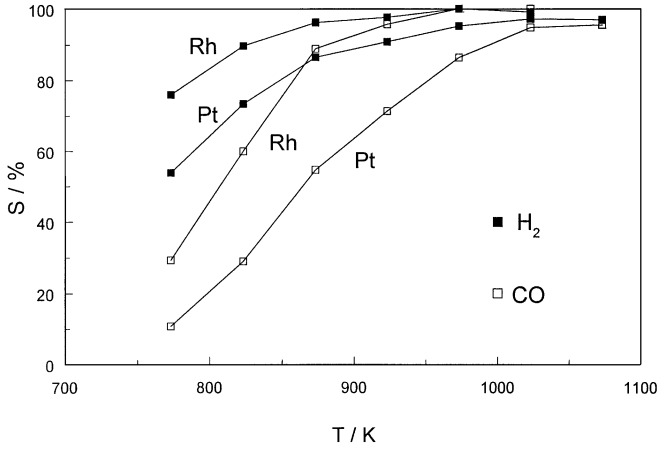

FIG. 10. Selectivity to CO and H_2 as a function of temperature for rhodium (0.4 wt% Rh_2O_3) and platinum sponge (0.9 wt% PtO_2). Continuous flow experiment of CH_4/O_2 at a feed molar ratio of 2. The oxygen conversion was complete in all experiments.

TABLE 2

Weight Percentages of Metal Oxide Present during the Simultaneous Interaction of Methane and Oxygen with Rhodium at 973 K and Platinum at 1023 K, as a Function of the Methane to Oxygen Feed Molar Ratio, Assuming an Oxide Stoichiometry of Rh_2O_3 and PtO_2

CH_4/O_2 Ratio	Rh_2O_3 (wt%)	PtO_2 (wt%)
0.5	2.1	2.9
1	0.6	1.5
2	0.4	0.9

0.5 were carried out. The total flow rate and the amount of surface platinum atoms are equal to that in the case of rhodium. Dioxygen was not detected quantitatively in any of the experiments nor were C_2-products observed. The carbon, hydrogen, and oxygen balances were always closed.

The results at a stoichiometric feed ratio are compared to that of rhodium in Figs. 9 and 10. The conversion of methane (Fig. 9) is always higher for rhodium compared to platinum in the temperature range of 800 K up to 1000 K. The selectivities of H_2 and CO (Fig. 10) are also higher for rhodium compared to platinum. At 773 K the difference in H_2 selectivity amounts to 22%, while that to CO amounts to 16%. At 923 K the difference in methane conversion between rhodium and platinum amounts to 15% and in the CO and H_2 selectivity 25 and 7%. At a temperature of 1000 K the selectivities to CO and H_2 are comparable.

At a feed molar ratio of 1 the conversion of methane increases from 75% at 773 K to 100% at 973 K. The selectivity to CO increases from 15 to 53% in the temperature range of 773 to 1023 K, while the corresponding selectivity to H_2 increases from 58 to 71%. At a feed molar ratio of 0.5 a complete conversion of methane to CO_2 and H_2O was observed in the temperature range of 773 to 1023 K.

The amount of platinum oxide, assuming a stoichiometry of PtO_2, was determined as a function of the feed molar ratio at a temperature of 1023 K. The results are presented in Table 2. The amount of PtO_2 present at reaction conditions increases with decreasing methane to oxygen molar ratio from 0.9 wt% at a stoichiometric feed ratio to 2.9 wt% at a feed molar ratio of 0.5 at a temperature of 1023 K. The first amounts to 48 theoretical monolayers of atomic oxygen.

DISCUSSION

Interaction of Dioxygen and Methane with Reduced Rhodium

Exposure of the reduced rhodium catalyst to a continuous flow of oxygen at 1073 K leads to the almost complete oxidation of the latter of Rh_2O_3.

The incorporation of oxygen during the multipulse experiments (Fig. 3) is attributed to the decomposition of the Rh_2O_3 phase at a pressure of 10^{-5} Pa and temperatures

in the range of 875 to 948 K. Contrary to platinum, dissolved oxygen species are not present, since no constant value is reached in the amount of incorporated oxygen as a function of the time of maintaining the oxidized catalyst at 10^{-5} Pa. Moreover, by interaction of dioxygen rhodium is almost completely oxidized, whereas platinum is oxidized only to an extent of 6 wt%. The decomposition rate of Rh_2O_3 is relatively slow since at a temperature of 948 K only an amount of oxygen equivalent to five theoretical monolayers is removed from the catalyst after a period of 900 s. The time scale of a typical TAP experiment amounts to 2 s and therefore the decomposition of Rh_2O_3 can be neglected during the simultaneous pulse experiments of methane and oxygen.

The shift of the peak maximum of the individual oxygen responses to a larger time value than that of the argon response (Fig. 4) is attributed to the reversible adsorption of oxygen at the catalyst surface. These species are assigned as dissociatively chemisorbed oxygen species, formed by the interaction of dioxygen with the catalyst surface. The time scale for desorption of the chemisorbed oxygen species amounts to 2 s.

The interaction of methane with reduced rhodium results in the formation of carbon adatoms and gaseous hydrogen. The apparent activation energy for methane decomposition of 15 kJ mol^{-1} is in reasonable agreement with the value of 21 kJ mol^{-1} reported by Brass and Ehrlich (42) for the dissociative chemisorption of methane on rhodium films.

Steady State of Rhodium at Temperatures and a Gas Composition Typical for Catalytic Partial Oxidation

Whereas the catalyst is almost completely oxidized to Rh_2O_3 in the presence of dioxygen alone, it is largely reduced during the simultaneous interaction of methane and oxygen at a stoichiometric feed ratio. The latter state corresponds to a steady state as indicated by the closed balances. Only 0.4 wt% Rh_2O_3 is present, equivalent to 10 theoretical monolayers of atomic oxygen. At decreasing methane to oxygen feed molar ratio, the percentage of Rh_2O_3 present increases.

A physical picture of a rhodium surface consisting of a matrix of metallic rhodium and islands of an oxide phase seems to be in line with literature results. The existence of a mixed phase, consisting of metallic Rh and Rh_2O_3 is reported by Peuckert (25) and is stable up to 800–850 K. The mixed phase may be represented as Rh_2O_3 clusters dispersed in a rhodium metal matrix. Salanov and Savchenko (21, 22) conclude that the formation of an island consisting of a surface oxide phase occurs at 500–700 K and thermal decomposition takes place at 750–900 K to yield dioxygen. Janssen *et al*. (43) studied the initial process of the oxidation of rhodium by field emission microscopy (FEM) and report formation of an oxide species on rhodium. This oxide species decomposes and oxygen desorbs between 800 and 1000 K. The oxidative process is reported to be surface-strcuture sensitive: the more open and rough the surface area, the more easy the oxidation.

Interaction of Methane with Chemisorbed Oxygen on Rhodium

The leveling off of the increasing selectivities of CO and H_2 from time intervals of 2 s between the pulsing of oxygen and methane onward (Fig. 5) indicates that chemisorbed oxygen is involved in the nonselective reaction paths of the partial oxidation of methane. Figure 6 shows that as soon as chemisorbed oxygen species are formed, the formation of CO_2 from CO increases. In the case of H_2 and H_2O a similar behavior is observed. These results indicate that chemisorbed oxygen species are involved in the consecutive oxidation of CO to CO_2 and H_2 to H_2O.

The absence of any carbon-containing product formation during an alternating pulse experiment starting with methane for time intervals longer than 0.5 s indicates that reactive carbon species with a long lifetime are not present on the surface as long as oxygen species are present.

Primary Product Formation on Rhodium

During the simultaneous interaction of methane and oxygen at a stoichiometric feed ratio (Fig. 8) the starting point and maximum of the H_2 response is observed prior to those of the response of H_2O. Similarly, the starting point and maximum of the CO response are observed prior to those of CO_2.

The order of appearance of H_2 and CO as well as H_2O and CO_2 as shown in Fig. 8 indicates that the former products are formed prior to the latter. One could argue that the order of appearance is determined by differences in Knudsen diffusion and adsorption/desorption coefficients. The order of appearance obtained by simulating the above phenomena for CO, H_2, H_2O, and CO_2 (see Fig. 1) corresponds to the order of appearance expected for a pulse experiment with CH_4 and O_2 with all four of the reaction products formed in a parallel way. The starting point and maximum of CO_2 is observed prior to that of CO. It follows from Fig. 8 that on the contrary during the simultaneous interaction of methane and oxygen the starting point and peak maximum of the CO response is observed prior to that of CO_2. It is concluded that CO is a primary reaction product. A similar conclusion is drawn for H_2 and H_2O, with hydrogen being the primary reaction product.

In the simulations the rate coefficients for adsorption and desorption of H_2, H_2O, and CO of Hickman and Schmidt (18) were used, which are valid for metal surfaces. In the present study a rhodium surface consisting of a matrix of metallic rhodium and islands of an oxide is proposed during the steady state at temperatures and gas composition typical for catalytic partial oxidation. However, it is assumed

that the surface is reduced in such a degree to allow the use of the rate constants of Hickman and Schmidt (18). During the simultaneous interaction of methane and oxygen at a stoichiometric feed ratio and closed balances, the direct formation of synthesis gas occurs. CO and H_2 are oxidized to CO_2 and H_2O via consecutive reaction paths.

Reaction Mechanism on Rhodium

The multipulse experiments of CH_4 and $^{18}O_2$ provide detailed information on the role of oxygen present as Rh_2O_3 versus chemisorbed oxygen in the partial oxidation of methane. During the first pulse, no formation of $C^{18}O$ was observed while $C^{16}O$ is being formed (Fig. 7), which means that formation of CO only proceeds via oxygen present as $Rh_2{}^{16}O_3$. The formation of $C^{16}O^{18}O$ and $C^{16}O_2$ during the first pulse indicates that both chemisorbed oxygen and $Rh_2{}^{16}O_3$ are involved in the consecutive oxidation of $C^{16}O$. Chemisorbed oxygen and $Rh_2{}^{16}O_3$ are both also involved in the consecutive oxidation of H_2, since formation of $H_2{}^{16}O$ as well as $H_2{}^{18}O$ is observed during the first pulse. The role of chemisorbed oxygen in the consecutive oxidation of CO and H_2 was already concluded from the alternating pulse experiments and is in line with the labeled oxygen experiment.

Only 5% of the total amount of ^{18}O pulsed in the first pulse is incorporated into the reaction products. The remainder of the ^{18}O is incorporated into the catalyst, which results in the formation of labeled rhodium oxide. As a result, the selectivity to $C^{16}O$ decreases and that to $C^{18}O$ increases at increasing pulse number (see Fig. 7).

Based on the experimental findings, the following reaction mechanism is proposed for the partial oxidation of methane over rhodium. Methane dissociates to carbon and hydrogen adatoms on reduced rhodium. It is assumed that the abstraction of H adatoms from CH_x species by O adatoms does not occur to a significant extent. This reaction would lead to the formation of OH species and finally to H_2O formation. However, the high selectivities to H_2 indicate that this is not a dominant reaction step. Oh *et al.* (44) proposed a mechanism for methane oxidation over alumina-supported noble metal catalysts in which O adatoms react with a CH_x species to form formaldehyde, which decomposes into CO and two H adatoms. The methane to oxygen feed ratio was varied between 0.2 and 1, and they report that the metal surface is predominantly covered with oxygen. This mechanism could account for primary formation of CO and H_2. However, no formation of formaldehyde was observed in the present study and the methane to oxygen feed ratio amounts to 2, resulting in a much lower oxygen coverage during the experiments.

The direct formation of CO from methane is believed to occur via a reaction between carbon adatoms and oxygen present as rhodium oxide. Hydrogen is formed as primary reaction product as well, via the associative desorption of two hydrogen adatoms from reduced rhodium. The consecutive oxidation of CO and H_2 occurs both via oxygen present as rhodium oxide and via chemisorbed oxygen.

Buyevskaya *et al.* (7) studied the partial oxidation of methane over 1 wt% $Rh/\gamma\text{-}Al_2O_3$. It was concluded that CO is a secondary product, formed by a surface reaction between carbon deposits and CO_2, which are the primary products. However, their response analysis is complicated due to the high specific surface area of their catalyst, 91 $m^2\ g^{-1}$ BET, which will influence the shape of the reponses due to diffusion in the pores of the catalyst. *In situ* DRIFTS studies performed on the same catalyts (8) led the authors to the conclusion that OH surface groups on the support are involved in the CH_x conversion to CO via a reforming reaction. Apparently, different results are obtained from experiments performed on a supported rhodium catalyst compared to the rhodium sponge of the present study. It is suggested that the $\gamma\text{-}Al_2O_3$ support is not inert at reaction conditions, but can especially catalyze the total oxidation reactions.

The observations of the present study are consistent with the following mechanism for the formation of synthesis gas over rhodium:

	σ	
$CH_4 + 5* \rightarrow C* + 4\,H*$	2	(1)
$C* + Rh_xO \rightarrow Rh_x^0 + CO + *$	2	(2)
$O_2 + 2\,Rh_x^0 \rightarrow 2\,Rh_xO$	1	(3)
$2\,H* \rightarrow H_2 + 2*$	4	(4)
$2\,CH_4 + O_2 \rightarrow 2\,CO + 4\,H_2;$		

here σ is the stoichiometric number.

The dissociation of methane, (Reaction 1) and the formation of H_2, (Reaction 4) are believed to occur on reduced rhodium sites. The formation of CO proceeds via a redox cycle postulated by Mars and van Krevelen (45) for selective oxidation reactions. The oxidation of the carbon adatoms to CO (Reaction 2) is accompanied by the reduction of rhodium oxide, which is reoxidized by incorporation of dioxygen into the catalyst (Reaction 3).

Comparison between Rhodium and Platinum

The partial oxidation of methane to synthesis gas over platinum has been reported upon previously (32) and is summarized below. On reduced platinum the decomposition of methane results in the formation of carbon and hydrogen adatoms. In the presence of dioxygen only, oxygen is present in three different forms: platinum oxide, dissolved oxygen, and chemisorbed oxygen species. CO and H_2 are produced directly from methane via oxygen present as platinum oxide. Activation of methane involving dissolved oxygen provides a parallel route to CO_2 and H_2O. Both platinum oxide and chemisorbed oxygen species are involved in the consecutive oxidation of CO and H_2. In the presence

of both methane and dioxygen at a stoichiometric feed ratio, dissolved oxygen species are not present and hence the dominant pathways are the direct formation of CO and H_2, followed by their consecutive oxidation. A Mars–van Krevelen redox cycle was postulated for the partial oxidation of methane over platinum.

The results of the continuous flow experiments of CH_4 and O_2 at a stoichiometric feed ratio (see Figs. 9 and 10) show that rhodium is a more active and selective catalyst than platinum at a comparable temperature. In the investigated temperature range the difference in the selectivity to CO is more pronounced than the difference in selectivity to H_2.

Hickman and Schmidt (15, 16) also observed a higher methane conversion over rhodium compared to platinum. Lapsewicz and Jiang (19) reported that methane activation is the rate-limiting step in the partial oxidation of methane. The difference in methane conversion can then be explained by the observed difference in apparent activation energy for methane activation on platinum, 52 kJ mol^{-1} (32), and rhodium, 15 kJ mol^{-1}.

Lapsewicz and Jiang (19) ascribe the observed differences in CO selectivity to the differences in ratios of surface species, such as oxygen, carbon, and hydrogen adatoms. Since the chemisorption of oxygen is not activated, the ability of the catalyst to activate methane determines the ratios of surface species. At increasing carbon to oxygen adatom ratio, the CO formation will be favored compared to the formation of CO_2 and a high hydrogen to oxygen adatom ratio is beneficial for the hydrogen selectivity. Hence, the differences in the selectivity to CO as well as H_2 observed in the present study can also be explained from the viewpoint that rhodium has a much lower activation energy than platinum for methane activation.

Contrary to the results of the present study, Hickman and Schmidt (15, 16) observed comparable selectivities to CO on Pt and Rh applying an autothermally operated reactor. The optimal selectivities are $S_{H_2} = 43\%$ and $S_{CO} = 89\%$ for the platinum catalyst compared to $S_{H_2} = 73\%$ and $S_{CO} = 90\%$ for the rhodium catalyst. The difference in the H_2 selectivity was explained by the higher activation energy for OH formation on Rh, 84 kJ mol^{-1}, compared to platinum, 11 kJ mol^{-1}. Therefore, on rhodium H adatoms are more likely to combine and desorb as H_2 than on Pt, which allows a faster formation of OH species. This reasoning may also provide an explanation for the higher H_2 selectivity of rhodium observed in the present study, in addition to the difference in the activation energy of methane activation. The discrepancy concerning the CO selectivity can be explained by the difference in mechanism. The balance between the rate of the oxidation and reduction steps determines the amount of metal oxide present at steady state. The lower amount of rhodium oxide present at steady state compared to platinum oxide at a stoichiometric feed ratio may explain the higher CO selectivity on rhodium since this could also correspond to a lower rate of the consecutive oxidation reaction of CO.

By interaction with dioxygen, rhodium is almost completely oxidized to Rh_2O_3 at 1073 K and the formation of this oxide phase was confirmed by *ex situ* XRD and XPS measurements. For platinum a maximum amount of oxide equivalent to 6 wt% PtO_2 was formed at 1023 K. However, the presence of a PtO_2 phase could not be confirmed by an *ex situ* XRD analysis. Dissolved oxygen species were not observed in the case of rhodium during the interaction with dioxygen, probably due to the almost complete oxidation of rhodium to Rh_2O_3.

During the simultaneous interaction of methane and oxygen the percentage of metal oxidized is larger for platinum than for rhodium (see Table 2). The difference is most pronounced at a stoichiometric feed ratio. In the steady state the amount of metal oxide results from the rate of metal oxidation by oxygen and the rate of oxide reduction by carbon adatoms. Hence, the differences between platinum and rhodium as shown in Table 2 may be explained by the lower activation energy for methane decomposition on rhodium, resulting in a higher concentration of carbon adatoms and thus a higher rate of oxide reduction.

CONCLUSIONS

During the interaction of dioxygen with rhodium sponge, the catalyst is almost completely oxidized to Rh_2O_3. In addition to rhodium oxide, oxygen is also present in the form of chemisorbed oxygen species. During the simultaneous interaction of methane and dioxygen at a stoichiometric feed ratio and a temperature of 973 K the catalyst is mainly in the metallic rhodium phase.

The decomposition of methane on reduced rhodium results in the formation of carbon and hydrogen adatoms. Synthesis gas is a primary product. Hydrogen is formed via the associative desorption of two hydrogen adatoms from reduced rhodium and the reaction between carbon adatoms and oxygen present as rhodium oxide results in the formation of carbon monoxide. The consecutive oxidation of CO and H_2 proceeds via both chemisorbed oxygen and oxygen present as rhodium oxide. A Mars–van Krevelen mechanism is postulated for the partial oxidation of methane over rhodium: methane reduces the rhodium oxide, which is reoxidized by dioxygen.

When compared to platinum, rhodium shows a higher methane conversion at a comparable temperature and also a higher selectivity to both CO and H_2. All differences are caused by the activation energy for methane decomposition which is higher on platinum than on rhodium. An additional explanation for the observed difference in the H_2 selectivity could be the higher activation energy for OH formation on rhodium compared to platinum.

APPENDIX: NOMENCLATURE

Roman Symbols

a_v	External catalyst surface area per unit catalyst volume ($m_c^2\ m_c^{-3}$)
A_s	Cross sectional area of the reactor (m_r^2)
C	Concentration (mol m_g^{-3})
d_i	Diameter of interstitial voids (m)
d_p	Particle diameter (m)
D_e^κ	Effective Knudsen diffusion coefficient ($m_g^3\ m_r^{-1}\ s^{-1}$)
k	Reaction rate coefficient (reaction dependent)
l_b	Bed length (m_r)
L_t	Maximal molar concentration per square meter catalyst surface (mol m_c^{-2})
M	Molecular mass (kg mol^{-1})
n	Total amount of moles (mol)
N_p	Amount of a component in inlet pulse (mol)
R	General gas constant (J $mol^{-1}\ K^{-1}$)
S	Selectivity (mol mol^{-1})
t	Time (s)
T	Temperature (K)
x	Axial coordinate in reactor (m)
X	Conversion (mol mol^{-1})

Greek Symbols

ε_b	Bed porosity ($m_g^3\ m_r^{-3}$)
τ_b	Bed tortuosity ($m_g^2\ m_r^{-2}$)
θ	Fractional coverage on the catalyst surface
ϵ	Mass balance (mol mol^{-1})
σ	Stoichiometric number
τ	Time scale (s)

Subscripts

A	With respect to A
ads	Adsorption
b	Bed; interstitial voids
des	Desorption
diff	Knudsen diffusion
$*$	Vacant sites

ACKNOWLEDGMENT

The financial support provided by the Commision of the European Union in the framework of the JOULE programme, subprogramme Energy from Fossil Sources, Hydrocarbons, No. JOU2-CT92-0073, is gratefully acknowledged.

REFERENCES

1. Prettre, M., Eichner, Ch., and Perrin, M., *Trans. Faraday Soc.* **43**, 335 (1946).
2. Dissanayake, D., Rosynek, M. P., Kharas, K. C. C., and Lunsford, J. H., *J. Catal.* **132**, 117 (1991).
3. Ashcroft, A. T., Cheetham, A. K., Foord, J. S., Green, M. L. H., Grey, C. P., Murrell, A. J., and Vernon, P. D. F., *Nature* **344**, 319 (1990).
4. Vernon, P. D. F., Green, M. L. H., Cheetham, A. K., and Ashcroft, A. T., *Catal. Lett.* **6**, 181 (1990).
5. Vernon, P. D. F., Green, M. L. H., Cheetham, A. K., and Ashcroft, A. T., *Catal. Today* **13**, 417 (1992).
6. Vermeiren, W. J. M., Blomsma, E., and Jacobs, P. A., *Catal. Today* **13**, 427 (1992).
7. Buyevskaya, O. V., Wolf, D., and Baerns, M., *Catal. Lett.* **29**, 249 (1994).
8. Walter, K., Buyevskaya, O. V., Wolf, D., and Baerns, M., *Cat. Lett.* **29**, 261 (1994).
9. Choudhary, V. R., Rajput, A. M., and Prabhakar, B., *Catal. Lett.* **15**, 363 (1992).
10. Choudhary, V. R., Rajput, A. M., and Prabhakar, B., *J. Catal.* **139**, 326 (1993).
11. Choudhary, V. R., Rajput, A. M., and Rane, V. H., *J. Phys. Chem.* **96**, 8686 (1992).
12. Choudhary, V. R., Rajput, A. M., and Rane, V. H., *Catal. Lett.* **16**, 269 (1992).
13. Choudhary, V. R., Sansare, S. D., and Mamman, A. S., *Appl. Catal.* **90**, L1 (1992).
14. Dissanayake, D., Rosynek, M. P., and Lunsford, J. H., *J. Phys. Chem.* **97**, 3644 (1993).
15. Hickman, D. A., and Schmidt, L. D., *Science* **259**, 343 (1993).
16. Hickman, D. A., Haupfear, E. A., and Schmidt, L. D., *Catal. Lett.* **17**, 223 (1993).
17. Hickman, D. A., and Schmidt, L. D., *J. Catal.* **138**, 267 (1992).
18. Hickman, D. A., and Schmidt, L. D., *AIChE J.* **39**, 1164 (1993).
19. Lapszewicz, J. A., and Jiang, X.-Z, *Prepr. Am. Chem. Soc. Div. Pet. Chem.* **37**, 252 (1992).
20. Matsumura, Y., and Moffat, J. B., *Catal. Lett.* **24**, 59 (1994).
21. Salanov, A. N., and Savchenko, V. I., *Surf. Sci.* **296**, 393 (1993).
22. Salanov, A. N., and Savchenko, V. I., *Kinet. Catal.* **34**, 478 (1993).
23. Salanov, A. N., and Savchenko, V. I., *React. Catal. Lett.* **49**, 29 (1993).
24. Salanov, A. N., and Savchenko, V. I., *Kinet. Catal.* **35**, 722 (1994).
25. Peuckert, M., *Surf. Sci.* **141**, 500 (1984).
26. Wang, T., and Schmidt, L. D., *J. Catal.* **71**, 411 (1981).
27. Carol, L. A., and Mann, G. S., *Oxid. Met.* **34**, 1 (1990).
28. Beck, D. D., Capehart. T. W., Wong, C., and Belton, D. N., *J. Catal.* **144**, 311 (1993).
29. Kellog, G. L., *Phys. Rev. Lett.* **54**, 1, 82 (1985).
30. Kellog, G. L., *Surf. Sci.* **171**, 359 (1986).
31. Oh, S. H., and Carpenter, J. E., *J. Catal.* **80**, 472 (1983).
32. Mallens, E. P. J., Hoebink, J. H. B. J., and Marin, G. B., *Catal. Lett.* **33**, 291 (1995).
33. Gleaves, J. T., Ebner, J. R., and Kuechler, T. C., *Catal. Rev.-Sci. Eng.* **30**, 49 (1988).
34. Huinink, J. P., Ph.D. Thesis, Eindhoven University of Technology, 1995.
35. Huizenga, D. G., and Smith, D. M., *AIChE J.* **32**, 1 (1986).
36. Schäfer, H., Tebben, A., and Gerhardt, W., *Z. Anorg. Allg. Chem.* **321**, 41 (1963).
37. Alcock, C. B., and Hooper, G. W., *Proc. Roy. Soc. A* **254**, 551 (1960).
38. Barin, I., "Thermochemical Data of Pure Substances." VCH, Weinheim, 1993.
39. Heuer, A. H., and Lou, V. L. K., *J. Am. Ceram. Soc.* **73**, 2785 (1990).
40. Lou, V. L. K., Mitchell, T. E., and Heuer, A. H., *J. Am. Ceram. Soc.* **68**, 49 (1985).
41. Barin, I., and Knacke, O., "Thermochemical Properties of Inorganic Substances." Springer-Verlag, Berlin, 1973.
42. Brass, S. G., and Ehrlich, G., *J. Chem. Phys.* **87**, 4285 (1987).
43. Janssen, N. M. H., van Tol, M. F. H., and Nieuwenhuys, B. E., *Appl. Surf. Sci.* **74**, 1 (1994).
44. Oh. S. H., Mitchell. P. J., and Siewert, R. M., *J. Catal.* **132**, 287 (1991).
45. Mars, P., and van Krevelen, D. W., *Chem. Eng. Sci.* **3**, 41 (1954).